ORIENTAL JOURNAL OF CHEMISTRY
An International Open Access, Peer Reviewed Research Journal
www.orientjchem.org
ISSN: 0970-020 X
CODEN: OJCHEG
2024, Vol. 40, No.(5):
Pg. 1470-1478

Improved Hydrogen De/Absorption Kinetics of Magnesium (Mg) *via* Addition of Catalyst Y_2O_3

MADHU YADAV[1,2], DEEPAK KUMAR YADAV[1,3], SATYA NARAYAN DOLIA[1,2] and CHHAGAN LAL[1,2*]

[1]Department of Physics, University of Rajasthan Jaipur, JLN Marg, Jaipur-302004 Rajasthan, India.
[2]Centre for Non-Conventional Energy Resources, University of Rajasthan Jaipur, JLN Marg Jaipur 302004 Rajasthan, India.
[3]Department of Physics, Government GNA PG College, Bhatapara, 493118, Chhattisgarh, India.
*Corresponding author E-mail: clsaini52@uniraj.ac.in, clsaini52@gmail.com

http://dx.doi.org/10.13005/ojc/400530

(Received: July 06, 2024; Accepted: September 13, 2024)

ABSTRACT

MgH_2 is attracting significant attention in the field of materials for storing hydrogen due to its mass-related hydrogen retention capacity, excellent reversibility, and cost-effectiveness making it a feasible option for fulfilling energy-sustaining needs. Despite its slow desorption and absorption limitation, the kinetics of MgH_2 can be improved by the ball milling technique. In this work to synthesis nanocomposite, various wt% concentrations of Y_2O_3 (X = 5, 10) are introduced to MgH_2. Thermodynamics of all prepared samples were measured by DSC, TGA, and PCT/PCI setups. The PCT investigation reveals that the Mg/MgH_2-5 wt% Y_2O_3 nanocomposites store 4.7 wt% H_2, where 100 h milled Mg/MgH_2 store 5.2 wt% hydrogen. Adding Y_2O_3 with MgH_2 reduces the dehydriding activation energy and onset temperature of Mg/MgH_2.

Keywords: Y_2O_3, PCT, DSC, TGA, MgH_2, Hydrogen storage, Activation energy.

INTRODUCTION

Hydrogen gets attenuation in the whole world due to its dense energy content of 142 MJ/kg, compact, ecofriendly nature, and can easily be produced from water[1]. The main problem associates with its storage, which makes it not suitable for automobile as well as industrial applications. Its liquid and gas phase storage required cryogenic and high-pressure storage tanks. Both methods have a very high explosion risk and large energy lose due to boiling off[2]. The main challenge of hydrogen storage is closely linked to the need for the development of reliable and efficient hydrogen compression methods. Solid-state hydrogen storage provides a much easier, safer, effective, and economical way to store hydrogen[3]. Throughout recent decades ammonia borane[4,5] lithium compounds[6,7], lightweight metal hydrides (for example MgH_2, $NaAlH_4$, $LiAlH_4$, LiH, $LaNi_5H_5$, $TiFeH_2$, PdH_2) have been considered for their role as solid state materials used for storing hydrogen[8].

In all above MgH_2 has shown great potential as a solid-state hydrogen storage media because of

its large hydrogen storage capacity (theoretical ~7.6 wt%), compact, most abounded element, low cost, and high reversibility[9,10]. Due to high thermal stability and poor ab/desorption kinetics, it is not widely used in both automotive and industrial applications[11]. In later times, several attempts have been made to enhance sorption kinetics and heat dynamics of Mg/MgH_2, such as ball milling, catalysts, and alloys as dopants. For example, materials such as metals[12-15], alloys[16-21], oxide[11,22–24], and halides[25-28], have been doped with Mg/MgH_2. Extensive research efforts have been dedicated to transitional metal oxides serving as efficient catalysts to store hydrogen in MgH_2. Oelerich *et al.,* reported that the catalysing impact of TiO_2, V_2O_5, Cr_2O_3, Mn_2O_3, Fe_3O_4, and CuO on the hydrogenation properties of Mg are comparable[29]. Fe_3O_4 demonstrated superior catalytic activity in the dehydrogenation reaction, which was succeeded by V_2O_5, Mn_2O_3, Cr_2O_3, and TiO_2. Remarkably, Barkhordarian *et al.,* recorded the exceptional catalytic activity of Nb_2O_5 and the rapid hydrogen sorption kinetics of 0.2 mol.% Nb_2O_5-doped Mg with nanosized crystal lattice[30].

Xueping *et al.,*[31] examine the catalytic role of Y_2O_3 in promoting the dehydrogenation of $NaAlH_4$. It was observed that hydrogen storage capacity rises with Y_2O_3 concentration. Where desorption rate firstly increases and then decreases with Y_2O_3 concentration. Furthermore, Liu *et al.,*[32] examined the hydrogenation properties of MgH_2-Y_2O_3/NiO hybrid. Their study revealed that the dehydrogenation temperature of MgH_2 reduces with an enhancement of Y_2O_3/NiO hybrid. They found that Y_2O_3 plays a superior role in enhancing hydrogen storage capacity, improving cycle life kinetics, and sorption kinetics of MgH_2. Surface reactivity of Y_2O_3 powder toward hydrogen has been studied by Kogler *et al.,*[33] and they found that due to the specific hydrophilicity of the oxide, sorption of water eventually takes place. The evidence supporting this surface-restricted mechanism is further strengthened by the absence of bulk structure and even at the highest reduction temperature (1173 K) morphological changes were observed upon reduction. To the authors' knowledge, the catalytic effect of Y_2O_3 on MgH_2 has not been widely studied so far. In the present study, we conducted a comprehensive study of catalytic role of Y_2O_3 on the hydrogen storage properties and sorption kinetics of Mg/MgH_2.

Experimental Preparation

Nano-Composite Preparation

Mg and Y_2O_3 powder of purity 99.98% were used during the synthesis procedure. Mg-x wt% Y_2O_3 (x = 0, 5, 10) powder was loaded into a ball milling jar and then sealed with an O ring. Whole process is carried into a glove box filled with pure argon gas. Then sealed jar was transferred to ball milling machine (Model: Retsch PM 100 type). Ball-Milling process was performed for 100 h at a speed of 150rpm. To synthesis Mg-x wt%Y_2O_3 nanocomposites, ball to charge ratio of roughly 5:1 was used. Ball-Milling procedure was performed at room temperature under atmospheric condition.

Structural and Morphological Characterization

Catalytic role on crystal structure and crystalline dimension were examined by using cu-kα radiation (λ=1.54 Å). XRD data was collected across the 20-80^{o}C range. The surface morphology of the synthesized samples was measured by Scanning electron microscope (SEM, Model Nova-Nano FE-SEM 450) at 15 kV. Chemical elemental composition was recorded by an EDX detector, which is inbuilt in SEM instrument.

Thermodynamics of Dehydrogenation

Thermodynamics of the hydrogen-depleting reaction of Mg and Mg-5 wt% Y_2O_3 nano-composites were measured via a Differential Scanning Calorimeter (DSC Model No. 7020). All DSC measurements were carried out at diverse heating rates of 5, 10, 15, and 20 0C/min in scale of thermal conditions 30^{0}C-550^{0}C. Roughly 5-6 mg sample was used for each DSC measurement. A constant nitrogen flow of 60 mL/min was maintained during the whole measurement.

Catalytic effect on dehydrogenation properties was carried out with Thermal Gravimetric Analyzer (TGA) measurement (STA Model Hitachi TGA-7300). Other Conditions are the same as of DSC measurement.

Pressure-Composition-Temperature analysis

A sievert-type Homemade PCI/PCT setup was employed to measure the hydrogen storage attributes of MgH_2-x wt% (x = 0, 5, 10). Roughly 1 g sample was used for each PCT measurement. Before every measurement, a leakage test was performed for 24 h at 350^{0}C. After that activation process was executed at 350^{0}C and 2 Mpa H_2 pressure for 6 h followed by 6 cycles of activation. After each sample loading the same process was repeated. Then PCT measurement was taken. Notably, Van't Hoff equation was used to measure the enthalpy and

entropy of re-hydrogenation reaction. Generally, enthalpy and entropy of most metal hydride are negative, except in certain instances.

RESULT AND DISCUSSION

Figure 1 represents the XRD spectrum of Mg/MgH_2 and Mg-5 wt% Y_2O_3 nanocomposites. XRD investigation reveals that the phase identity of Mg/MgH_2 and Mg-5 wt% Y_2O_3 is maintained during ball milling. XRD spectrum indicates the existence of diverse phases within the nanocomposites, which possibly occur during ball-milling. The presence of these phases provides extra catalytic effects on the hydrogenation properties of Mg-5 wt% Y_2O_3 nanocomposites. XRD data revealed diminished peak intensities and stretching of the Full width at half maxima (FWHM), value MgH_2 is 0.17, and for Mg+5 wt%Mg+Y_2O_3 is 0.2 signifying the presence of physical stress accumulation and reduction in particle dimension during ball milling. Ball-milling creates new active surfaces, resulting in enhanced hydrogenation properties of the nanocomposite. Analysing, the X-ray diffraction (XRD) spectra focus on the full width at half maxima (FWHM) and peak intensity, which are essential parameters for assessing crystallinity and grain size. A narrower FWHM signifies larger crystallite sizes and improved crystallinity, as broader peaks usually indicate smaller crystallites or greater structural disorder. Higher peak intensity reflects better crystallinity and larger grain sizes, indicating well-aligned and abundant crystalline planes. The lattice parameters for MgH_2 and Mg+5 wt%Mg+Y_2O_3 are as for MgH_2 a=b=4.49 Å &C=2.0 Å and for Mg+5 wt%Mg+Y_2O_3 are a = b = c= 10.606 Å as verified from JCPDS file no.-01-079-6694 and JCPDS file no.-01-089-5592.

These values align well with previously reported data. The ratio c/2a lattice parameter for MgH_2 is 0.22 and for Mg+5 wt%Mg+Y_2O_3 is 0.5.

The crystallite size D was determined using Scherrer's formula:

$$D = \frac{k\lambda}{\beta cos\theta}$$

Where D is the average crystallite size, k is the shape factor, λ is the wavelength of Cu-Kα X-rays, β is the full width at half maxima (FWHM), θ is the Bragg angle. The value of D for MgH_2 is 79nm and for Mg+5 wt%Mg+Y_2O_3 is 71.5nm.

By calculating, the dimensions of dislocation lines per unit volume, the dislocation density(δ) is calculated using Williamson and Smallman's formula is

$$\delta = \frac{1}{D^2}$$

The value for MgH_2 is 0.00016 nm^{-2} and for Mg+5 wt% Mg+Y_2O_3 is 0.00019 nm^{-2}.

Unit Cell Volume (V)

The unit cell volume V for MgH_2 was calculated using the relation $V = a^2 c$ and Mg+5 wt% Mg+Y_2O_3 is calculated by $V = a^3$, where a and c are the lattice parameters values are 40.3202 $Å^3$ and 1193.03 $Å^3$.

Microstrain (ε)

Stress is an important factor influencing the structural features of crystalline lattices when there is a geometric mismatch between their boundaries. The relationship illustrated below can be utilized to compute microstrain (ε).

$$\epsilon = \frac{\beta cos\theta}{4}$$

The value for MgH_2 is 0.043855nm and for Mg+5 wt% Mg+Y_2O_3 is 0.04845nm.

Then, it is summarised as MgH_2 has a slightly larger crystallite size, lower dislocation density, and larger unit cell volume than MgH_2-5 wt% Y_2O_3. A slight peak shift for (110) was measured for MgH_2 with the addition of Y_2O_3. And two peaks of Y_2O_3 for the plane (222) and (431) was noted.

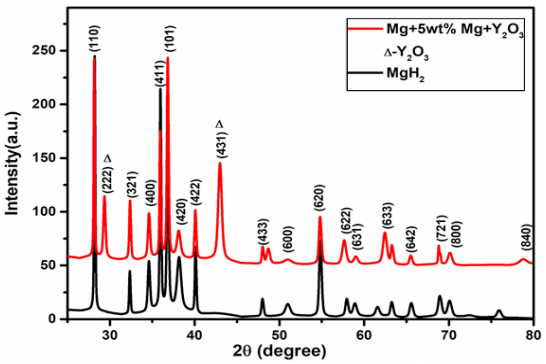

Fig. 1. XRD spectrum of 100 h milled MgH_2 and Mg-5 wt% Y_2O_3 nanocomposites

SEM (Scanning electron Microscopy)

Surface morphology of all synthesis

samples is shown in Fig. 2. Fig. 2(a) represents the SEM micrograph of 100 h milled MgH_2 and 2(b) represents MgH_2- 5 wt%Y_2O_3 nanocomposites. The average crystalline size for MgH_2 was recorded at ~79nm and for MgH_2- 5 wt% Y_2O_3 nanocomposites was in the range of ~71.5nm. SEM imaging indicates a decrease in the particle size after ball milling, generating a refreshed surface area conducive to hydrogen absorption and release within the composites. Examination of SEM images shows that ball milling yields a nonuniform particle size distribution. Analysis of SEM images emphasize the dense aggregation of small particles in the vicinity of large particles and some clusters are present in the prepared samples. This property plays an important role in improving the kinetics of hydrogenation. Fig. 2(c) and 2(d) represents the EDX mapping of 100 h milled MgH_2 and MgH_2-5 wt%Y_2O_3 nanocomposites. The EDX analysis provides information on both elemental identification and quantitative composition. Hight of the peaks represents the chemical quantitive information of the nanocomposites.

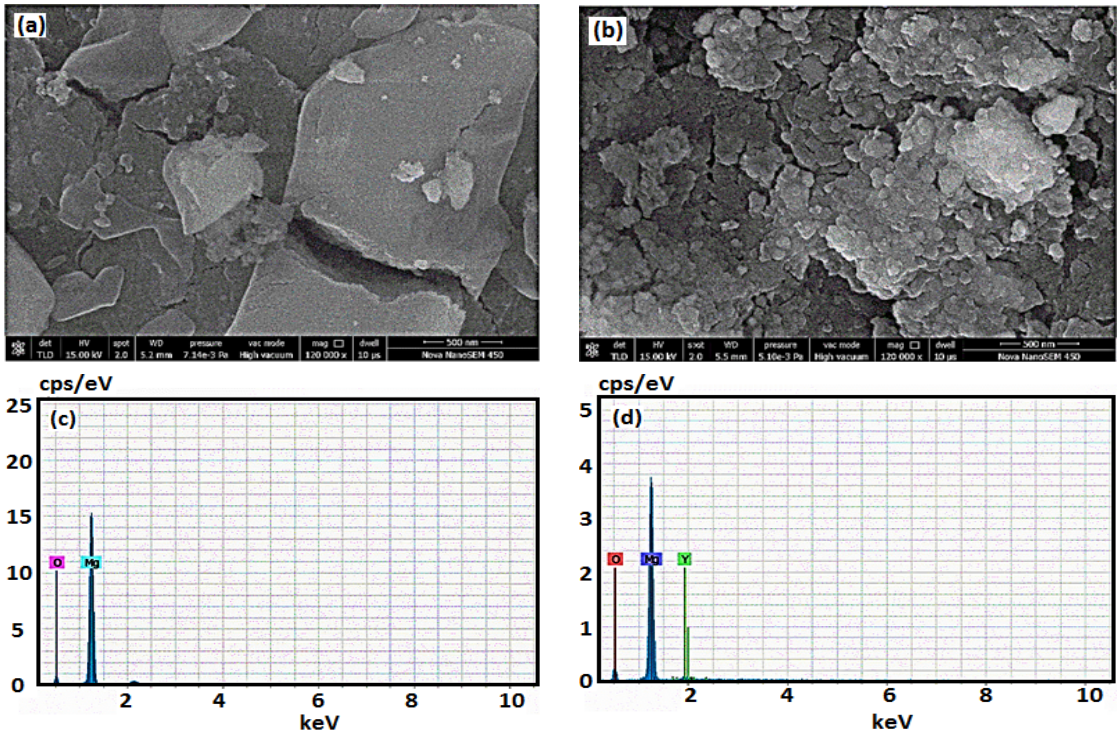

Fig. 2. FE-SEM for 100 h milled (a) MgH_2 (b) for Mg-5 wt% Y_2O_3 nanocomposites, EDX graphing for 100 h milled (c) MgH_2 (d) for Mg-5 wt% Y_2O_3 nanocomposites

Figure 3 represent particle size distribution of MgH_2 and MgH_2-5 wt% Y_2O_3 nanocomposites. For each plot about 200 data points have been recorded. The average particle size found for MgH_2 is 81.963 ± 32.045nm and for MgH_2-5 wt% Y_2O_3 is 81.021 ± 21.273nm.

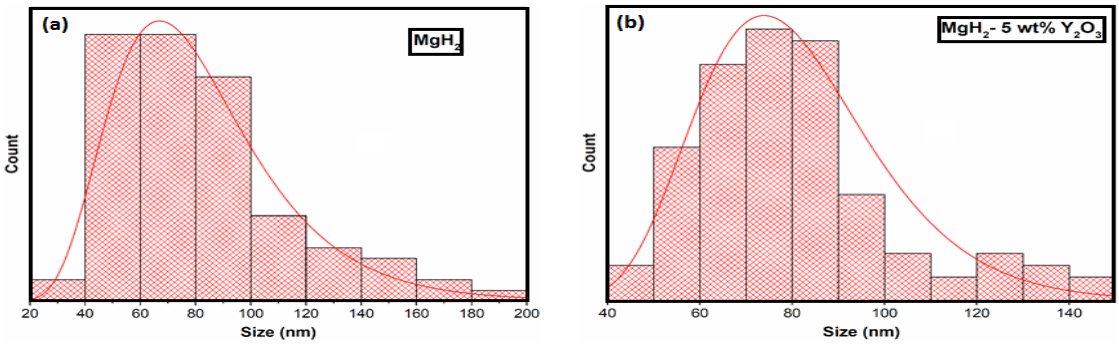

Fig. 3. Particle size distribution plots of 100 h milled (a) MgH_2 and (b) MgH_2-5 wt% Y_2O_3

Pressure-Composition-Temperature

Pressure-composition-temperature is carried out at diverse temperatures for 100 h milled Mg and Mg-5 wt% Y_2O_3. The maximum hydrogen absorption achieved for Mg is 5.2 wt% at 320°C as shown in Fig. 4(a). The results indicate that as temperature increases, the plateau pressure shifts towards the higher end, correlating with a decrease in absorption capacity, and notably the plateau pressure does not persist unchanged with the temperature.

Fig. 4(b). Represents the maximum absorption capacity achieved for Mg-5 wt% Y_2O_3 nanocomposites is 4.7 wt% at 280°C. The PCT plot recorded in the temperature range 280-340°C. PCT investigation indicate that with the increase of temperature absorption capacity reduces. But the plateau pressure didn't persist unchanged with the temperature.

Fig. 4(c). Shows comparative study at temperature 280°C at different weight percentage. So, it shows that Mg-5 wt%Y_2O_3 have higher hydrogen absorption capacity as compare to different weight percentage. From the PCT analysis it is clear that as we increase Y_2O_3 concentration absorption capacity of Mg/MgH_2 reduces.

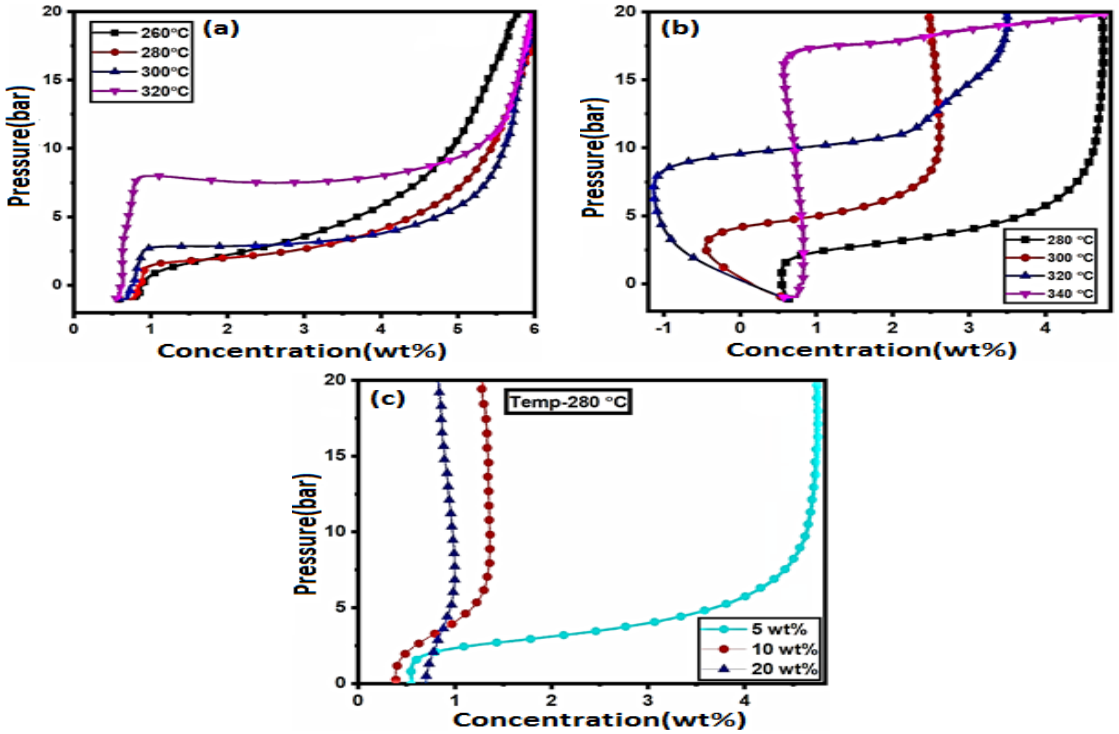

Fig. 4. Shows PCT profile of (a) 100 h milled Mg/MgH_2, (b) Mg-5 wt% Y_2O_3 nanocomposites, and (c) Comparative study at different wt%

Enthalpy and entropy for hydrogenation reaction were determined applying the Van't Hoff equation to PCT measurements and analyzing by Van't Hoff plots. Fig. 5 represents the Van't Hoff plot of 100 h milled (a) Mg/MgH_2 (b) Mg-5 wt% Y_2O_3, and the calculated enthalpy and entropy for MgH_2 is 52.502 kJ/mol and 104.25 J/mol-k, for Mg-5 wt% Y_2O_3 is 76.995 kJ/mol and 149.236 J/mol-K, and for Mg-10 wt% Y_2O_3 is 55.156 kJ/mol and 108.976 J/mol-K respectively. So, from the results we conclude that the lowest enthalpy was obtained for Mg-5 wt% Y_2O_3 nanocomposites. Entropy calculations are conducted to understand the transition from gaseous molecular hydrogen to dissolved atomic hydrogen. Enthalpy governs the heat released or absorbed during hydrogen uptake or release reaction.

Thermodynamics and Kinetics of the dehydrogenation process

TGA and DSC analysis of MgH_2 and Mg-5 wt% Y_2O_3 nanocomposites at different heating rates

are shown in Fig. 6(a, b). Thermogravimetric analysis (TGA) of MgH_2 shows that the maximum weight loss is observed at 15°C/min and loss is reached up to 3.1% at 460°C and Mg-5 wt% Y_2O_3 shows that the maximum weight loss is 1.6% up to 477°C at the heating scale of 20°C/min.

Thermodynamics analysis of Mg and Mg-5 wt% Y_2O_3 nanocomposites were examined through Differential Scanning Calorimetry as shown in Fig. 6(c, d). The decomposition of metal hydride often leads to an exothermic reaction. The exothermic reaction represents the hydrogen is liberated through the decomposition of MgH_2 at 449°C at the heating scale of 15°C. As, the heating rate decreases the peak shifted towards lower side. Heat flow profile obtained by the Mg-5 wt% Y_2O_3 show decomposition at 447°C at the heating scale of 20°C. With decreasing heating rate, the peak tends to move towards lower end. DSC and TGA analysis indicate that on set temperature of Mg/MgH_2 shifted toward lower end with increasing Y_2O_3 concentration.

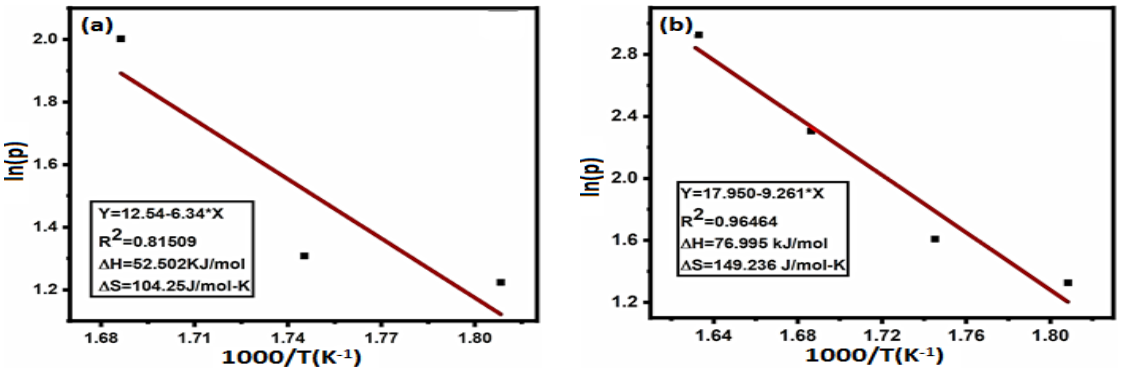

Fig. 5. Van't Hoff Plot of 100 h milled (a) Mg/MgH_2, (b) Mg-5 wt% Y_2O_3 nanocomposites

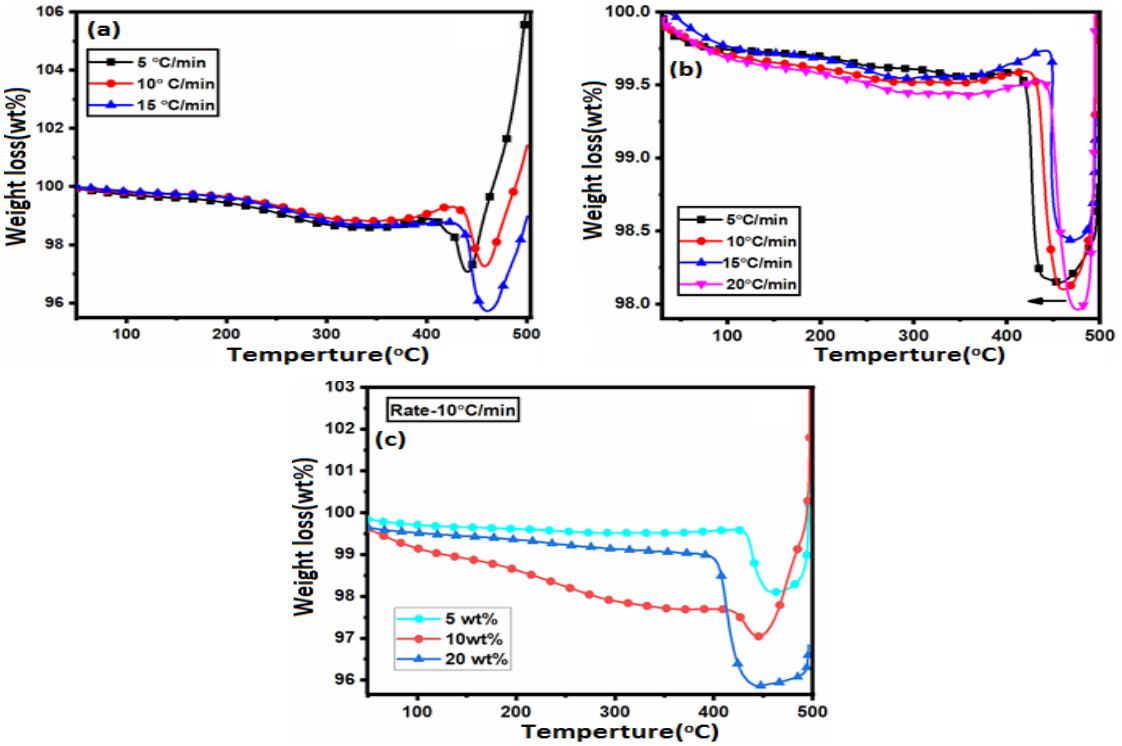

Fig. 6(a, b). Shows TGA for 100 h milled MgH_2 and Mg-5 wt% Y_2O_3 nanocomposites (c) shows comparative study at the rate of 10°C/min

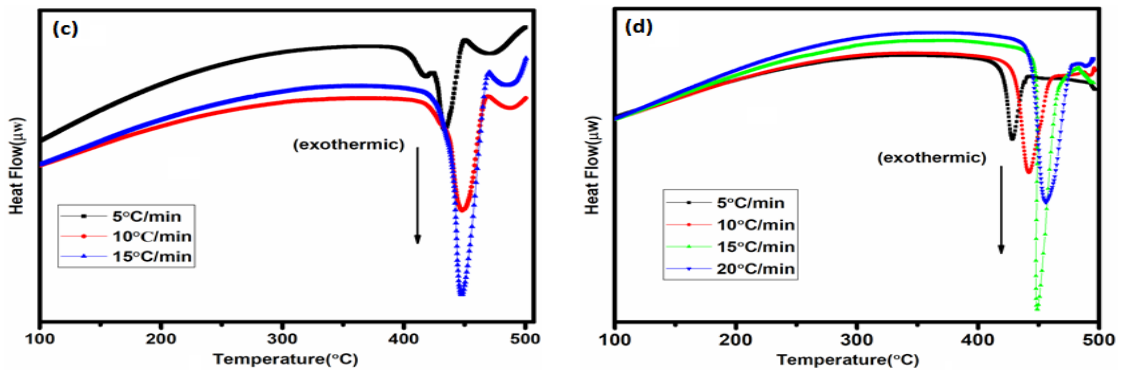

Fig. 6(c, d). Shows DSC for 100 h milled MgH_2 and Mg-5 wt% Y_2O_3 nanocomposites

The activation energy for dehydrogenation reaction of the synthesized nanocomposites has been derived. By performing TGA measurements at varying heating rates under the correspondent experimental setup, the activation energy can be determined using Kissinger equation.

$$lnk = -\frac{E_a}{RT_p} + \alpha\alpha$$

Where $k=\beta/T_p^2$, β represents the heating rate, T_P represents the peak temperature, R represents the gas constant and E_a represents the activation energy. When plotting a graph of ln(k) contrary to 1/T, slope corresponds to $-E_a/R$. The activation energy value is accumulated from the slope. Fig. 7 shows activation energy for (a) MgH_2 and (b) Mg-5 wt% Y_2O_3. The calculated activation energy for MgH_2 is 218.57 kJ/mol and for Mg-5 wt% Y_2O_3 is 203.03 kJ/mol. The activation energy acts as threshold that must be surpassed to initiate the liberation of hydrogen and its nanocomposites. Fig. 7 illustrates decrease of activation energy with catalyst concentration. The behavior affected by factors such as catalytic impact, particle dimension, surface area, and catalytic properties affects the desorption rates. Sample with higher activation energy are indicative of heightened thermal stability.

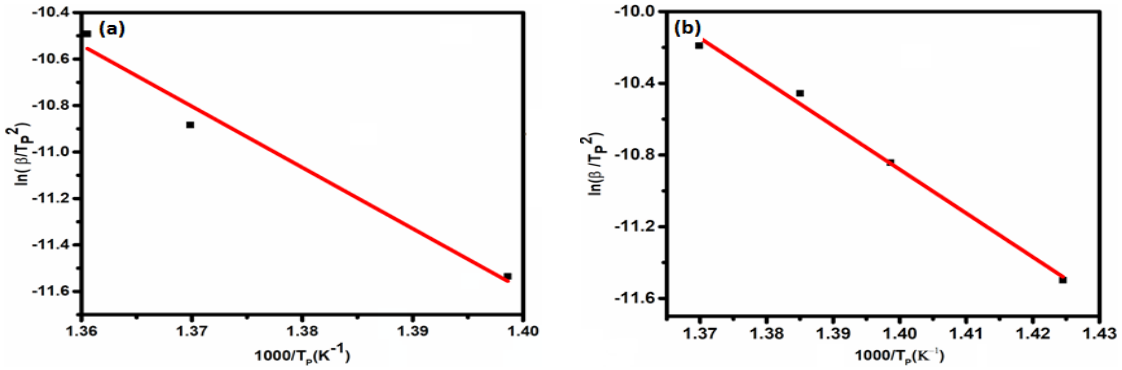

Fig. 7. Kissinger plot of 100 h milled (a) MgH_2, and (b) for Mg-5 wt% Y_2O_3 nanocomposites

CONCLUSION

The study focused on examination how catalysts Y_2O_3 influence structural, morphological, and ab/desorption kinetics of Mg/MgH_2 by utilizing XRD, FE-SEM with EDX and simultaneous TGA-DSC techniques. XRD and SEM investigation shows that ball-milling provides non-uniform mixing and creates new active fresh surface, which leads to increase hydrogen ab/desorption kinetics as well as capacity of Mg/MgH_2. PCT analysis revels that the highest absorption achieved for Mg/MgH_2 is at 5.2 wt% at 320°C and for Mg-5 wt% Y_2O_3 nanocomposites is 4.04 wt% at 280°C. From PCT analysis it is clear that that the hydrogen absorption capacity of Mg/MgH_2 reduces with increasing Y_2O_3 concentration. The DSC analysis indicates that that the decomposition of metal hydride often leads to an exothermic

reaction. Through the decomposition of MgH_2 hydrogen is liberated at 449°C and Mg-5 wt% Y_2O_3 shows decomposition at 447°C. DSC analysis revels that the onset hydrogenation temperature of Mg/MgH_2 shifted towards lower end with addition of Y_2O_3 catalyst. TGA analysis shows that activation energy for MgH_2 is 218.57 kJ/mol and for Mg-5 wt% Y_2O_3 is 203.03 kJ/mol. So, by the addition of catalysts activation energy decreases.

ACKNOWLEDGMENT

The authors would like to acknowledge the Department of Physics, University of Rajasthan, Jaipur for their assistance with TGA and DSC facilities respectively. Also thankful to MNIT Jaipur for Characterization XRD and FE-SEM with EDX facility.

Conflicts of interest

No conflicts to be disclosed

REFERENCES

1. Chawla, K.; Yadav, DK.; Sharda, P.; Lal, N.; Sharma, S.; Lal, C., *International Journal of Hydrogen Energy*., **2020**, *45*(44), 23971-23976.
2. Chawla, K.; Yadav, DK.; Bajpai, A.; Kumar, S.; Lal, C., *Environmental Science and Pollution Research*., **2021**, *28*, 3872-3879.
3. Sakintuna, B.; Lamari-Darkrim, F.; Hirscher, M., *International Journal of Hydrogen Energy.,* **2007**, *32*(9), 1121-1140.
4. Hu, MG.; Geanangel, RA.; Wendlandt, WW., *Acta*., **1997**, *23*, 249-255.
5. Stephens, FH.; Pons, V.; Baker, RT.; *Dalton Trans*., **2007**, doi:10.1039/B7030532C.
6. Chen, P.; Xiong, Z.; Luo, J.; Lin, J.; Tan, KL., *Nature*., **2002**, *420*, 302–304.
7. Chen, P.; Xiong, Z.; Luo, J.; Lin, J.; Tan, KL., *Journal Phys. Chemsitry.* B., **2003**, *107*, 10967–10970.
8. Jain, I.; Jain, P.; Jain, A., *Journal Alloy Compound.,* **2010**, *503*(2), 303-39.
9. Schlapbach, L.; Zuttel, A., *Nature*., **2001**, *414*, 353-358.
10. Jain, IP.; Lal, C.; Jain, A., *International, Journal Hydrogen Energy*., **2010**, *35*, 5133-5144.
11. Yadav, DK.; Chawla, K.; Jain, IP.; Lal, C., *Environmental Science and Pollution Research.,* **2021**, *28*, 3866-3871.
12. Ouyang, LZ.; Cao, ZJ.; Wang, H.; Liu, JW.; Sun, DL.; Zhang, QA.; Zhu, M., *International Jounral Hydrogen Energy.,* **2013**, *38*, 8881-8887.
13. Hanad, N.; Ichikawa, T.; Fujii, H., *Journal, Phys. Chemistry* B., **2005**, *109*, 7188-7194.
14. Dai, J.H.; Song, Y.; Yang, R., *Journal Phys. Chemistry* C., **2010**, *114*, 11328-11334.
15. Mahmoudi, N.; Kaflou A.; A. Simchi A., *J. Power Sources*., **2011**, *196*, 4604-4608.
16. Zhong, H. C.; Wang, H.; Ouyang, L. Z., *International Journal Hydrogen Energy*., **2014**, *39*, 3320-3326.
17. Yu, X. B.; Yang, Z. X.; Liu, H. K.; Grant, D. M.; Walker, G. S., *International Journal Hydrogen Energy*., **2010**, *35*, 6338-6344.
18. Janot, R.; Darok, X.; Rougier, A.; Aymard, L.; Nazri, G. A.; Tarascon, J. M., *Journal Alloys Compound.,* **2005**, *404-406*, 293-296.
19. Chawla, K.; Sharma, G.; Bajpai, A.; Roy, P.K.; Jain, I.P.; Lal C., *International Journal of Hydrogen Energy*., **2024**, *57*, 1253-1262.
20. Chawla, K.; Yadav, D.K.; Bajpai, A.; Jain, I.P. and Lal, C., *Sustainable Energy Technologies and Assessments*., **2022**, *51*, 101981.
21. Friedrichs, O.; Aguey-Zinsou F.; Ares Fernandez J. R.; Sanchez-Lopez J. C.; Justo A.; Klassen T.; Bormann R.; Fernandez A., *Acta Materialia*., **2006**, *54*, 105-110.
22. Révész, A.; Fátay, D.; Zander, D.; Spassov, T., *Journal of Metastable & Nanocrystalline Materials*., **2015**, *24-25*, 447-450.
23. Cabo, M.; Garroni, S.; Pellicer, E.; Milanese, C.; Giella, A.; Marini, A.; Rossinyol, E.; Surinach, S.; Baro, M.D., *International Journal Hydrogen Energy*., **2011**, *36*, 5400-5410.
24. Yadav, D. K.; Chawla, K.; Lal, N.; Choudhary, B. L.; Lal, C., *Materials Today: Proceedings*., **2021**, *46*, 2326-2329.
25. Yavari, A. R.; Le Moulec, A.; Castro F. R. D.; Deledda, S.; Friedrichs, O.; Botta, W. J.; Vaughan, G.; Klassen, T.; Fernandez, A.; Kvick, A., *Scripta Materialia*., **2005**, *52*, 719-724.

26. Jin, S. A.; Shim, J. H.; Cho, Y. W.; Yi, K. W., *J. Power Sources*., **2007**, *172*, 859-862.
27. S. Kumar.; A. Jain.; S. Yamaguchi.; H. Miyaoka.; T. Ichikawa.; A. Mukherjee.; G. K. Dey.; Y. Kojima., *Int. J. Hydrogen Energy*., **2017**, *42*, 6152-6159.
28. Ismail, M., *Energy*., **2015**, *79*, 177-182.
29. Oelerich, W.; Klassen, T.; Bormann, R., *J Alloys Compd*., **2001**, *315*, 37-42.
30. Barkhordarian, G.; Klassen, T.; Bormann, R., *Scr Mater*., **2003**, *49*, 213-217.
31. Xueping, Z.; Guo, X.; Shenglin, L.; Xin, F. and Jiaojiao, Z., Effect of CeO_2 and Y_2O_3 as Catalysts on Hydrogen Desorption Properties of $NaAlH_4$., *Rare Metal Materials and Engineering*., **2013**, 42(7),1321-1324.
32. Liu, Y.; Wang, S.; Li, Z.; Gao, M.; Liu, Y.; Sun, W.; Pan, H., *Processes*., **2021**, *9*(5), 892.
33. Kogler, M.; Köck, E.M.; Bielz, T.; Pfaller, K.; Klötzer, B.; Schmidmair, D.; Perfler L.; Penner S., *The Journal of Physical Chemistry* C., **2014**, *118*(16), 8435-8444.